

Article

Residual Repeated Impact Strength of Concrete Exposed to Elevated Temperatures

Raad A. Al-Ameri ¹, Sallal R. Abid ^{2,*} , G. Murali ³, Sajjad H. Ali ² and Mustafa Özakça ¹

¹ Department of Civil Engineering, Gaziantep University, Gaziantep 27310, Turkey; raada.alameri@gmail.com (R.A.A.-A.); ozakca@gantep.edu.tr (M.Ö.)

² Department of Civil Engineering, Wasit University, Kut 52003, Iraq; sajhali.wasit@gmail.com

³ School of Civil Engineering, SASTRA Deemed University, Thanjavur 613401, India; murali@civil.sastra.edu

* Correspondence: sallal@uowasit.edu.iq

Abstract: Portland cement concrete is known to have good fire resistance; however, its strength would be degraded after exposure to the temperatures of fire. Repeated low-velocity impacts are a type of probable accidental load in many types of structures. Although there is a rich body of literature on the residual mechanical properties of concrete after high temperature exposure, the residual repeated impact performance of concrete has still not been well explored. For this purpose, an experimental study was conducted in this work to evaluate the effect of high temperatures on the repeated impact strength of normal strength concrete. Seven identical concrete patches with six disc specimens each were cast and tested using the ACI 544-2R repeated impact setup at ambient temperature and after exposure to 100, 200, 300, 400, 500 and 500 °C. Similarly, six cubes and six prisms from each patch were used to evaluate the residual compressive and flexural strengths at the same conditions. Additionally, the scattering of the impact strength results was examined using three methods of the Weibull distribution, and the results are presented in terms of reliability. The test results show that the cracking and failure impact numbers of specimens heated to 100 °C reduced slightly by only 2.4 and 3.5%, respectively, while heating to higher temperatures deteriorated the impact resistance much faster than the compressive and flexural strengths. The percentage reduction in impact resistance at 600 °C was generally higher than 96%. It was also found that the deduction trend of the impact strength with temperature is more related to that of the flexural strength than the compressive strength. The test results also show that, within the limits of the adopted concrete type and conducted tests, the strength reduction after high temperature exposure is related to the percentage weight loss.

Keywords: repeated impact; ACI 544-2R; high temperatures; fire; residual strength



Citation: Al-Ameri, R.A.; Abid, S.R.; Murali, G.; Ali, S.H.; Özakça, M. Residual Repeated Impact Strength of Concrete Exposed to Elevated Temperatures. *Crystals* **2021**, *11*, 941. <https://doi.org/10.3390/cryst11080941>

Academic Editors: Cesare Signorini, Antonella Sola, Sumit Chakraborty and Valentina Volpini

Received: 14 July 2021

Accepted: 10 August 2021

Published: 12 August 2021

Publisher's Note: MDPI stays neutral with regard to jurisdictional claims in published maps and institutional affiliations.



Copyright: © 2021 by the authors. Licensee MDPI, Basel, Switzerland. This article is an open access article distributed under the terms and conditions of the Creative Commons Attribution (CC BY) license (<https://creativecommons.org/licenses/by/4.0/>).

1. Introduction

Repeated accidental impact is a type of unfavorable load that most building structures are not designed to withstand. Impact loads are a type of short-term dynamic load that exposes the material to unusual and unwanted stresses, which is more effective on brittle materials such as concrete. Repeated impacts occur due to the accidental falling of building materials during the construction period, or other objects during the life span, from higher stories [1–3]. In parking garages, the collision of cars can also be a source of repeated impacts on columns and walls. Other example sources are repeated hits by projectiles or explosive shrapnel in conflict regions [4,5]. The evaluation of the influence of repeated impacts on the material microstructure and the residual performance of the structural members requires an adequate evaluation of the cracking and fracture behavior under such type of loads. Pre-evaluation of material behavior under repeated impacts can be conducted using the ACI 544-2R [6] repeated drop weight impact test, which can be considered as the simplest and cheapest impact test to evaluate the impact performance of concrete [7–9].

This test was used to evaluate the impact performance of several types of concrete mixtures by several recent researchers.

Concrete is a type of cementitious material that is composed mainly of Portland cement and aggregate that are mixed with water to form a moderately low cost construction solution with a sufficient compressive strength [10–13]. Although there have been great advances in the branch of material science and the development of many evolutionary modern types of concrete that possess seriously superior strength and ductility characteristics by incorporating new fiber-reinforced cementitious composites, normal weight, normal strength Portland cement-based concrete is still the most widely used type in reinforced concrete buildings [14,15]. Concrete structures, as with other structure types, are always under the danger of accidental fires that may occur due to electrical issues or inconvenient occupation. With the existence of furniture, fires can reach temperatures as high as 1000 °C in a very short period. Yearly, tens of thousands of fires are reported in countries such as the USA and the UK, 40% of which are classified as structural fires [16]. Although concrete is considered a good fire-resistant material, exposure to high temperatures with a steep temperature increase would seriously deteriorate the concrete structural members [15,17]. Due to the low thermal conductivity of concrete and considering the quick temperature increase, high temperature gradients would form between the exposed surfaces, the cores and the opposite unexposed surfaces [18]. Such gradients would induce internal thermal stresses on the microstructural scale, leading to steep material degradation [19,20]. The non-uniform thermal movements (expansion) of the different material parts owing to the non-uniform thermal gradients, and the chemical decomposition of calcium hydroxide beyond 400 °C [19,21–23] would initiate the effective degradation of the strength until failure.

Three main types of fire test procedures have been used by researchers to simulate the strength reduction in the material under high temperature exposure, two of which simulate the conditions of the concrete strength during fire exposure for compression and flexural members. In the first of these tests, which is the stressed fire test, the setup simulates the performance of compression members such as columns or compression parts of beams where the member is stressed by approximately 20% to 40% of its strength [24–26]. In this test, the specimens are preloaded to a constant stress level and then heated to the desired level of temperature, at which the temperature is kept constant to assure an approximately zero thermal gradient in the material (temperature saturation to the steady state condition). Then, the load is increased to failure. The second test is usually termed as the unstressed condition, which follows the same procedure of the first test setup but without preloading. This test simulates the conditions of beams and slabs where the concrete is usually under low tensile stresses [25]. On the other hand, the residual unstressed test is the third fire test setup. This test setup simulates the post-fire evaluation of the strength, where the specimens are heated unstressed to the required temperature, saturated at this temperature for a constant period and then cooled to ambient temperature. Finally, the cooled specimens are tested at ambient temperature to examine the residual strength of the concrete after the fire is over. The post-fire exposure strength evaluation is essential to decide whether the building is still functional, requires strength rehabilitation due to being unsuitable or must be demolished. Previous studies [25] showed that if the specimens are cooled in water (as in the case of water distinguishing a fire), the strength deteriorates at faster rates than when cooled under air convection. The volume changes resulting from the re-hydration (with cooling water) of dehydrated calcium silicate after exposure to temperatures higher than 400 °C have a destructive influence on the concrete microstructure [26].

Few research works are available in the literature about the evaluation of the concrete impact strength after high temperature exposure, most of which investigate high-strain rate impact tests and blast tests [27–31], while a very limited number of works were found on low-velocity impact tests on reinforced concrete members [18,32]. Most of these works developed numerical analyses to evaluate the dual effect of high temperature and high-strain rate impacts on reinforced concrete and composite structural members [33–35].

Although the combined action of fire exposure and low-velocity repeated impacts is probable in many structures such as parking garages, the authors could not find sufficient literature works that tried to explore the post-fire repeated impact performance of concrete. Mehdipour et al. [18] conducted an experimental study to evaluate the residual mechanical properties of concrete containing recycled rubber as a replacement of coarse aggregate, metakaolin as a partial replacement of Portland cement and steel fibers. Among the investigated mechanical properties, the authors evaluated the residual repeated impact strength using the ACI 544-2R test after exposure to temperatures of 150, 300, 450 and 600 °C. The test results showed that high temperature could significantly affect the residual cracking and failure impact numbers, where only one impact could cause the cracking of specimens heated to 600 °C. They also reported that a multi-surface cracking was observed for heated specimens instead of the central circular fracture of unheated fibrous specimens.

The current research investigated the impact resistance of normal concrete to low-velocity repeated impacts after exposure to high temperatures of accidental fires. As reviewed in the previous sections, such scenario is possible along the span life of concrete structures, while the number of studies on this topic is seriously limited. Aiming to fill the gap in knowledge in this area, a research program was initiated starting with the most usual concrete type in reinforced concrete structures, which is normal weight, normal strength concrete.

2. Experimental Work

As stated previously, the experimental work presented in this study was conducted to be a reference work for future works where the post-fire residual impact performance of fibrous concretes will be assessed. Therefore, a normal plain concrete mixture was adopted in this study to investigate the effect of repeated low-velocity impacts on heated concrete. A cement content of 410 kg/m³ was used with 215 kg/m³ of water, while the fine and coarse aggregate contents were 787 and 848 kg/m³, respectively. Local crushed gravel and river sand from Wasit Province, Iraq, were used as coarse and fine aggregates. The maximum size of the crushed gravel was 10 mm. The chemical composition and physical properties of the used cement are listed in Table 1, while the gradings of both the sand and gravel are shown in Figure 1. All specimens were cured for 28 days in temperature-controlled water tanks.

Table 1. Physical properties of cement.

Oxide (%)	Content
SiO ₂	20.08
Fe ₂ O ₃	3.6
Al ₂ O ₃	4.62
CaO	61.61
MgO	2.12
SO ₃	2.71
Loss on ignition (%)	1.38
Specific surface (m ² /kg)	368
Specific gravity	3.15
Compressive strength 2 days (MPa)	27.4
Compressive strength 28 days (MPa)	46.8

The impact tests were conducted using the standard ACI 544-2R repeated impact procedure. However, instead of the manual operation of the test, an automatic impact machine was built for this purpose and used in this study to perform the repeated impact tests. The impact machine shown in Figure 2a was built to reduce the efforts and time of the test, where repeated impacts were automatically applied using the standard ACI 544-2R drop weight (4.54 kg) and drop height (457 mm), while the crack initiation and failure were observed using a high-resolution camera, as shown in Figure 2b. The same standard test setup was followed, where a steel ball was placed on the top of the 150 mm-diameter

and 64 mm-thick disc specimen, while the drop weight fell directly on the steel ball that transferred it to the center of the specimen's top surface, as shown in Figure 2c. Once the first surface crack appeared, the number of repeated impacts was recorded, which is termed as the cracking number (N_{cr}). After, the impact was continued until the failure of the specimens, where the failure number (N_f) was recorded.

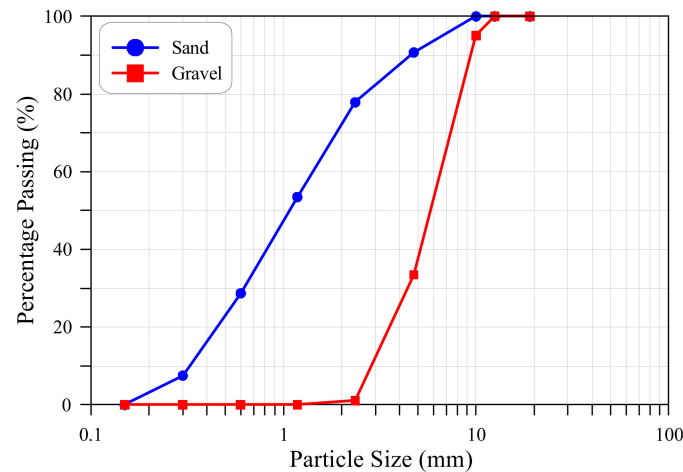


Figure 1. Grading of fine and coarse aggregates.

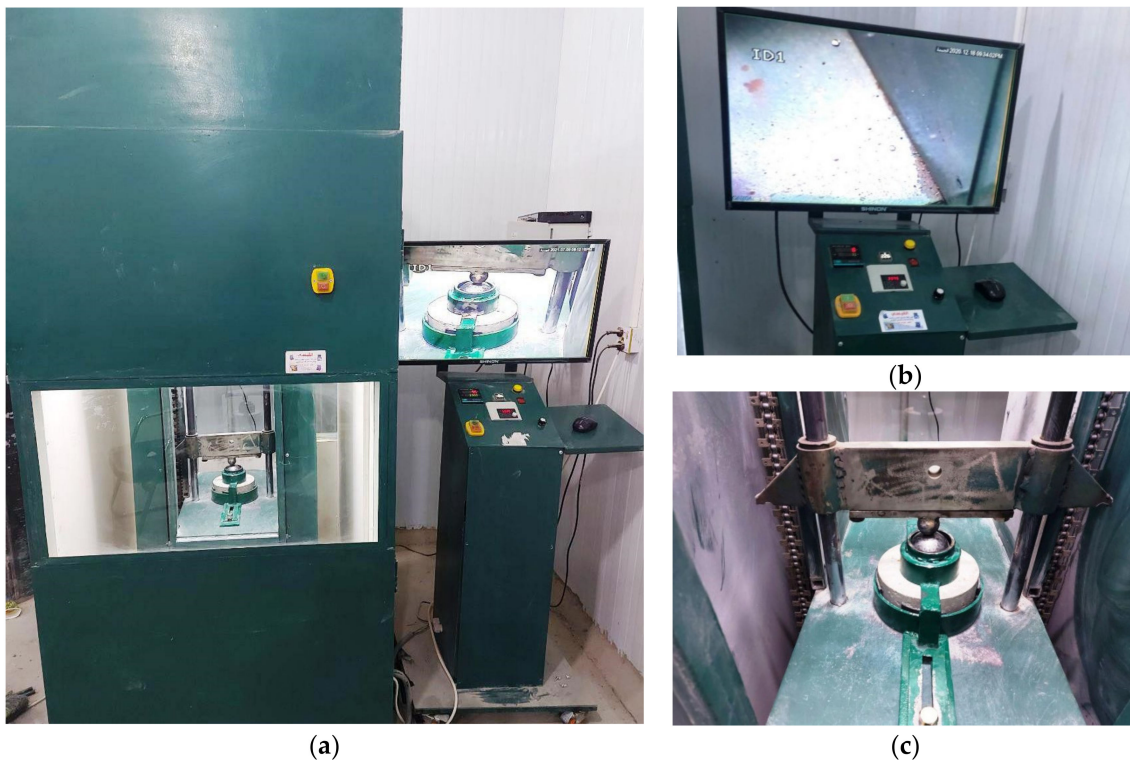


Figure 2. The automatic repeated impact testing machine (a) the impact machine; (b) crack observation; (c) the impact load and holding system.

In addition to the six impact disc specimens, six 100 mm cube specimens and six $100 \times 100 \times 400$ mm prisms were cast from the same concrete patches, as shown in Figure 3. The concrete cubes were used to evaluate the compressive strength, while the prisms were used to evaluate the modulus of rupture. Previous researchers [36] showed that increasing the size of the cube specimen from 100 to 150 mm had no significant effect on the residual compressive strength after exposure to temperatures up to $1200\text{ }^{\circ}\text{C}$, while others [37]

draw a similar conclusion for concrete cylinders having different sizes (diameter \times length) of 50 \times 100 mm, 100 \times 200 mm and 150 \times 300 mm. The cylinders were exposed to temperatures up to 800 °C. Several previous studies [38–46] adopted 100 mm cubes to evaluate the residual compressive strength of concrete.



Figure 3. Single group of disc, cube and prism specimens.

Seven concrete patches were cast and cured in water tanks under the same conditions for 28 days, after which the specimens were left to air dry for a few hours and then dried in an electrical oven at 100 °C for 24 hours [15,47–50]. After the specimens were naturally air cooled, six of the seven patches were heated to temperatures of 100, 200, 300, 400, 500 and 600 °C using the electrical furnace shown in Figure 4a, while the seventh patch was left as an unheated reference. As shown in Figure 4b, a steel cage was used to reduce the destructive effects of the concrete explosive failure on the internal walls and heaters of the furnace. The heating process followed the heating and cooling procedure shown in Figure 5, where the specimens were heated steadily at a heating rate of approximately 4 °C/min until the target temperature. After, the specimens were thermally saturated at this temperature for one hour to assure the thermal steady state condition [51,52]. Finally, the furnace door was opened to allow for the natural air cooling of the specimens, which were left in the laboratory environment and tested the next day.



(a)



(b)

Figure 4. The electrical furnace (a) furnace interiors; (b) specimens heating.

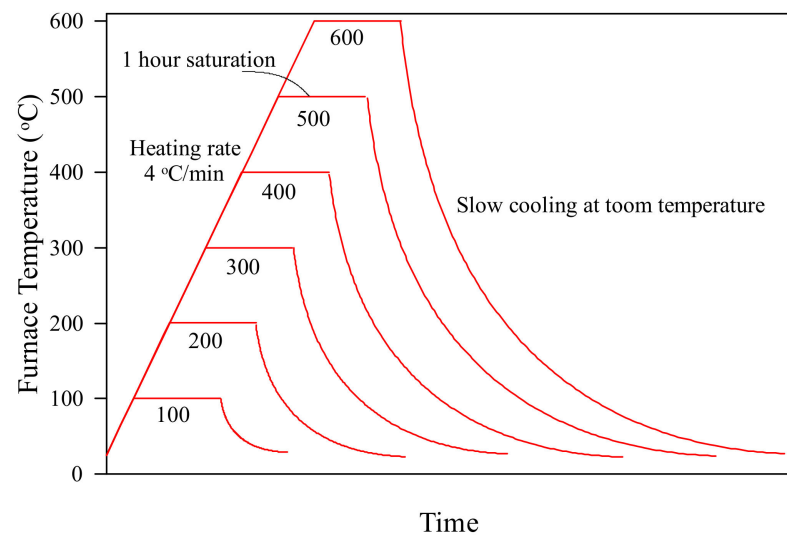


Figure 5. Heating and cooling regime of the electrical furnace.

The heating rate can affect the residual strength of concrete exposed to temperatures exceeding 300 °C [53]. Previous researchers used different heating rates to evaluate the residual properties of concrete, which were as low as 0.5 °C [54] and 1 °C [55] and as high as 30 °C [56]. However, heating rates ranging from 2 to 10 °C were the most common in the literature [57], where a heating rate of 2 °C was adopted by [58,59], while 3 °C was adopted by [60,61], and 4 °C was adopted by [62,63]. On the other hand, 5 °C was used by [64–67], and 6 °C and 7 °C were used by [38,64,68], while other previous researchers [69–71] used a heating rate of 10 °C. In this study, a heating rate within this range, 4 °C, was adopted.

3. Results and Discussion

3.1. Compressive Strength

The residual compressive strength values after exposure to 100, 200, 300, 400, 500 and 600 °C in addition to those at ambient temperature are shown in Figure 6. The figure also shows the percentage reduction in strength due to temperature exposure. It is obvious that a slight strength gain of approximately 1.5% was recorded at 100 °C, where the compressive strength after exposure to this temperature was 43.9 MPa, which is higher than that before heating (43.2 MPa). This initial strength gain was reported by previous researchers [25] and is attributed to the increase in the material density due to the evaporation of free pore water and the increase in hydration products owing to the accelerated pozzolanic reaction [72,73]. The strength gain is represented as a negative percentage reduction in Figure 6. After exposure to 200 °C, the compressive strength recorded 35.1 MPa, with a percentage reduction of approximately 18.8%, while a noticeable percentage strength recovery was recorded at 300 °C. The residual compressive strength at 300 °C was 42.3 MPa, and the percentage reduction was only approximately 2.1%. Hence, more than 16% of strength recovery was gained as the temperature was increased from 200 to 300 °C. As the temperature increased beyond 200 °C, the removal of water from the surfaces of the cement gel particles induced higher attraction surface forces (van der Waals forces), which might increase the ability of the microstructure to absorb higher compression stresses [18,73]. Beyond 300 °C, the compressive strength exhibited a continuous decrease in strength, with an increase in temperature, where the percentage strength reductions were 18.8, 22.4 and 50.0% after exposure to 400, 500 and 600 °C. The significant strength drop after 500 °C is attributed to the volume changes that took place due to the shrinkage of the cement paste and expansion of the aggregate particles, which deteriorate the bond between the two materials [25,74,75]. The dehydration of cement and decomposition of calcium hydroxide also lead to destructive effects [76,77].

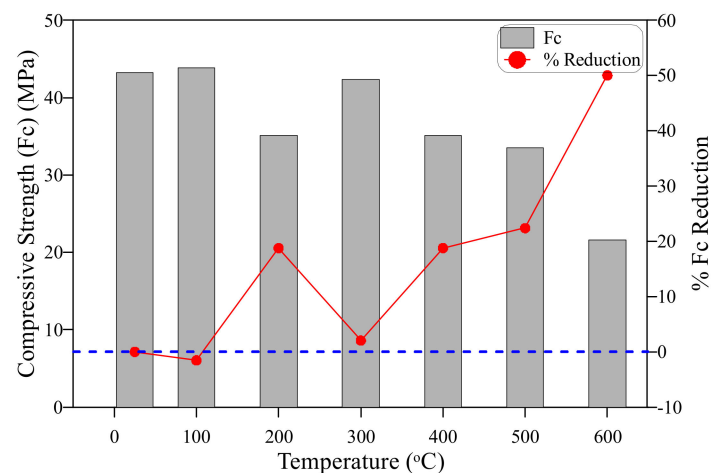


Figure 6. Compressive strength and its percentage reduction at different temperatures.

Figure 7 shows the relationship between the compressive strength and percentage weight loss of the same cube specimens after exposure to high temperatures of 100 to 600 °C. The percentage weight loss was calculated by dividing the weight loss (weight before heating-weight after heating) by the original specimen weight before heating, with the result multiplied by 100. The figure shows that three stages can be recognized in the percentage weight loss relation with temperature. In the first stage, the slope of the percentage weight loss was high after exposure to the sub-high temperature range (100 to 300 °C), which indicates early high weight loss. This weight loss can be attributed to the evaporation of the free pore water before 200 °C and the absorbed water in the cement gel particles. The second stage, which is a semi-stabilization stage with a very small positive slope, is related to the strength recovery and low reduction between 300 and 500 °C, where the microstructure is still not very affected by the chemical and physical changes due to temperature exposure. Finally, the weight loss starts another high-slope reduction region after 500 °C, where the cement matrix was cracked owing to the chemical changes, and the bond between the cement and aggregate was almost lost due to the different thermal movements [78,79]. Excluding the initial strength gain at 100 °C and the strength recovery at 300 °C, it can be said that the strength loss can be related to the loss in weight. The differences between strength loss and weight loss at these regions are attributed to the different behaviors of concrete under the different applied stresses, where it is stated that the residual tensile strength of concrete, for example, has a different behavior with temperature than that of the compressive strength. As weight loss is a stress-free measurement, there would be some expected differences with load tests.

3.2. Flexural Strength

The residual flexural strength records (modulus of rupture) of the tested prisms are visualized in Figure 8, which also visualizes the percentage reduction in flexural strength as a ratio of the unheated strength. The figure explicitly shows that a similar strength gain to that of the compressive strength was recorded for the flexural strength at 100 °C. However, the percentage increase was higher, where the unheated flexural strength was 3.7 MPa, while that after exposure to 100 °C was approximately 4.1 MPa, with a percentage increase of approximately 10.1%, which is depicted in Figure 8 as a negative percentage reduction. The same reason discussed in the previous section for the compressive strength could be the source of this increase in the flexural strength. After, a continuous strength deterioration was recorded as the temperature increased beyond 100 °C, where the residual modulus of rupture values were approximately 2.9, 2.4, 2.2, 1.6 and 0.3 MPa with respective percentage reductions of approximately 22.5, 35.1, 41.6, 57.3 and 91.2 % after exposure to 200, 300, 400, 500 and 600 °C. It can be noticed that the strength recovery recorded for the compressive strength at 300 °C was not recorded for the flexural strength, which

reflects the positive effect of physical attraction forces at this temperature to sustain higher compressive stresses, while such effect was insignificant under the flexural tensile stresses. Another result that was noticed is the faster deterioration of the flexural strength compared to the compressive strength, which is directly related to the weak microstructural response of concrete to tensile stresses. A similar flexural strength reduction behavior was reported by many previous works [25,72,80].

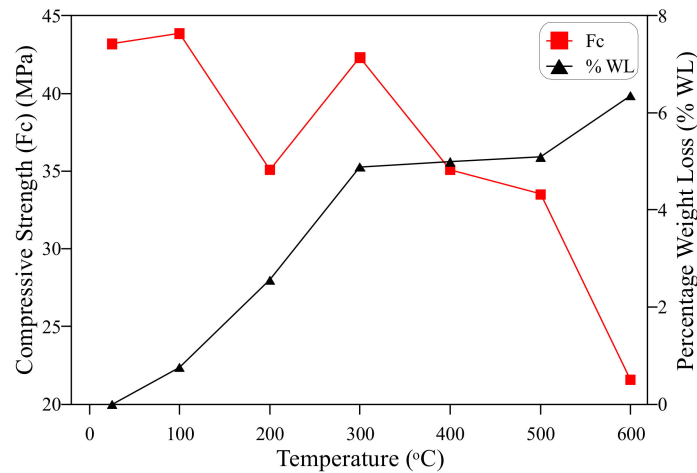


Figure 7. The relation of compressive strength and percentage weight loss of the cube specimens at different temperatures.

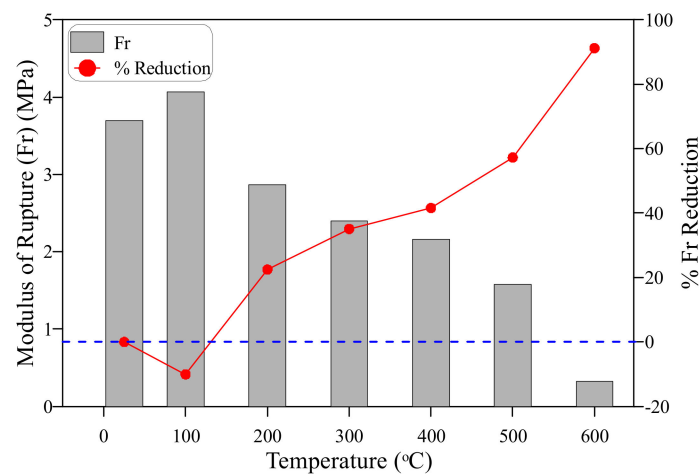


Figure 8. Flexural strength and its percentage reduction at different temperatures.

The weight loss for the same prisms was recorded, from which the percentage weight loss was calculated, which is depicted in Figure 9 against the residual modulus of rupture. The figure shows that a similar three-stage behavior can be recognized for the prism specimens to that recorded for the cube specimens, where the slope of the percentage weight loss was higher before 300 °C and beyond 500 °C, while it was lower between them. Similarly, excluding the high residual flexural strength recorded at 100 °C, the strength reduction curve exhibited a similar three-slope behavior to that of weight loss, where the percentage reduction slope was high from 100 to 300 °C and from 500 to 600 °C, while it was semi-stabilized between 300 and 400 °C for both the flexural strength and weight loss, as shown in Figure 9. This similar trend confirms the strong relation between weight loss and strength reduction after high temperature exposure.

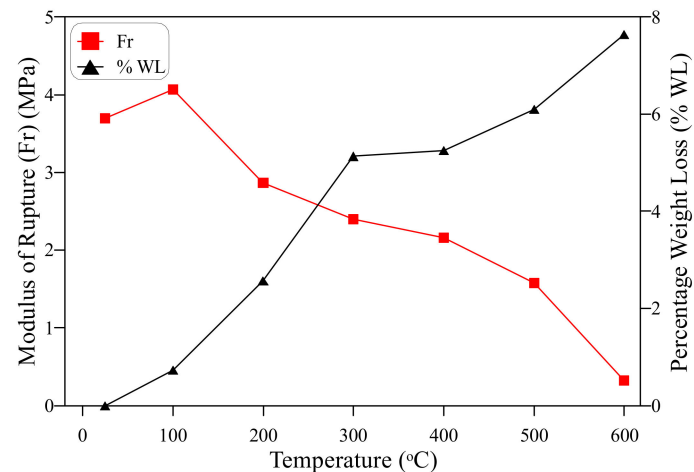


Figure 9. The relation of flexural strength and percentage weight loss of the prism specimens at different temperatures.

3.3. Repeated Impact Strength

This section presents and discusses the obtained results from the conducted drop weight repeated impact tests that were carried out at ambient temperature and after exposure to different levels of high temperatures. The results of all specimens are listed in Table 2 together with the mean, standard deviation (SD) and coefficient of variation (COV) of each of the six disc samples. It is obvious that for all specimens, before and after exposure to high temperature, the recorded failure number was slightly higher than the cracking number, which reveals the brittle nature of normal concrete under impact tests [81–83].

Table 2. Results of repeated impact test.

Temperature	R	100 °C		200 °C		300 °C		400 °C		500 °C		600 °C		
		N_{cr}	N_f											
1	52	53	28	29	18	19	8	9	4	5	2	3	1	2
2	41	42	76	78	25	26	7	8	2	3	2	3	1	3
3	78	81	41	43	11	12	6	7	4	5	2	3	1	2
4	50	53	90	91	9	10	7	8	3	4	3	4	1	2
5	51	54	39	41	9	10	4	5	2	3	1	2	1	2
6	58	60	48	49	13	14	7	8	3	4	3	3	1	2
Mean	55.0	57.2	53.7	55.2	14.2	15.2	6.5	7.5	3.0	4.0	2.2	3.0	1.0	2.2
SD	12.5	13.0	24.0	24.0	6.3	6.3	1.4	1.4	0.9	0.9	0.8	0.6	0.0	0.4
COV %	22.8	22.8	44.8	43.5	44.3	41.4	21.2	18.4	29.8	22.4	34.7	21.1	0.0	18.8

3.3.1. Cracking and Failure Impact Numbers

The detailed impact numbers are listed in Table 2, while Figures 10 and 11 show the post-high temperature exposure response of the cracking (N_{cr}) and failure (N_f) impact numbers, respectively. Figure 10 shows that after exposure to 100 °C, the cracking number was not noticeably affected, where this number was decreased from 55 to 53.7, with a percentage decrease of only 2.4%. Similarly, N_f was decreased by no more than 3.5%, as illustrated in Figure 11. Considering the known high variation in the ACI 544-2R repeated impact test [6], it can be said that the impact resistance was not affected by heating to 100 °C, which is also confirmed by the comparison of the individual impact numbers in Table 2, where the retained impact numbers for some specimens were higher after exposure to 100 °C than before heating. For instance, a cracking impact number of 90 was recorded for specimens heated to 100 °C, which is higher than all recorded numbers before heating. As discussed in the previous sections, the compressive strength and flexural

strength were increased after exposure to a temperature of 100 °C. The strength gain is reported to be due to the shrinkage of the concrete pore holes after the evaporation of the pore water, which resulted in denser media. The slow preheating of specimens in an electrical oven at 100 °C might also help to minimize the reduction in the impact strength at this temperature, where the free pore water was partially evaporated during the initial heating phase, resulting in the stress being relieved during the second (furnace) quick heating phase, which maintained the microstructural deterioration at a minimum. It should be mentioned that the oven's slow preheating is essential to prevent any type of thermal explosive failure during heating, which would be harmful to the furnace and other specimens in the furnace. The preheating process was a typical procedure followed by many experimental studies in the literature, where it was reported that thermal explosive spalling is probable at temperatures in the range of 300 to 650 °C [25].

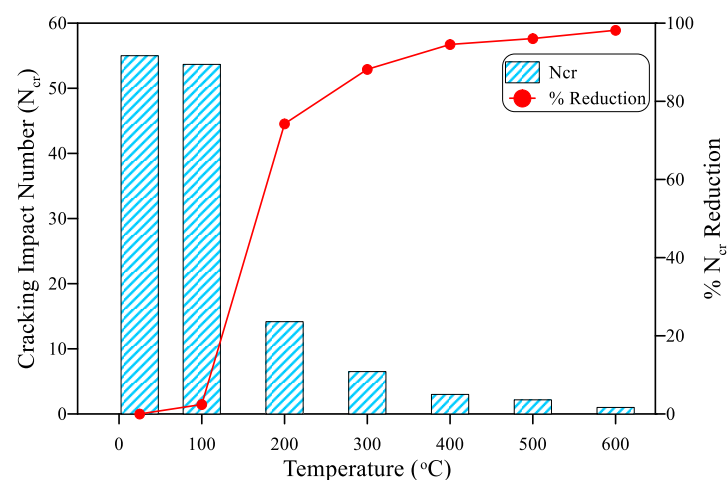


Figure 10. Cracking impact number and its percentage reduction at different temperatures.

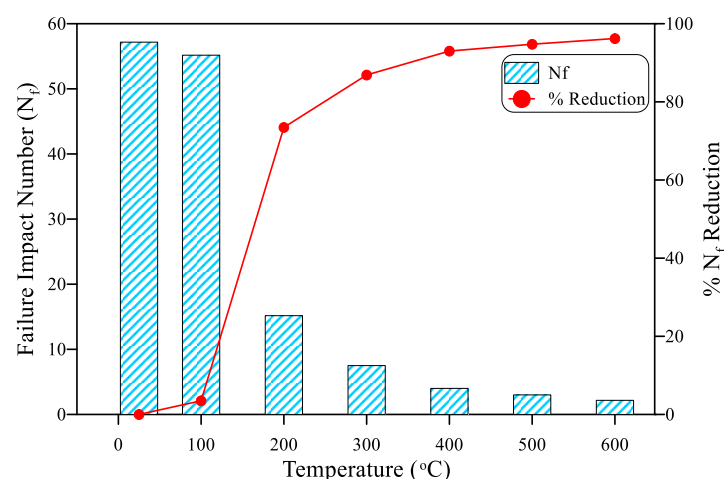


Figure 11. Failure impact number and its percentage reduction at different temperatures.

The strength of the material to resist impact forces dropped sharply after exposure to 200 °C, where the loss in impact resistance in terms of N_{cr} and N_f reached 74.2 and 73.5%, respectively. This reduction is dramatic and is much higher than the losses in the compressive, flexural and tensile strengths according to the literature and the current study results, where previous studies showed that the normal compressive strength range of normal concrete after exposure to 200 °C falls between 70 and 110% of the unheated strength [18,21,72]. Similarly, it is widely addressed in the literature that the modulus of elasticity of normal concrete would be higher than 70% of the unheated values [73–75].

Phan and Carino [25] reported that, for the case of an unstressed residual compressive strength test, which was the heating procedure followed in this research, an initial strength gain or minor loss is the usual trend of normal concrete up to 200 °C. The residual impact strength of the higher temperatures followed the same excessive strength drop, as shown in Figures 10 and 11. The residual cracking impact strength after exposure to 300, 400, 500 and 600 °C was, respectively, 11.8, 5.5, 3.9 and 1.8% of the original unheated strength. Similarly, the residual failure impact strengths were 13.1, 7.0, 5.2 and 3.8% after exposure to 300, 400, 500 and 600 °C, respectively. Two points should be discussed here, namely, the strength reduction behavior with temperature, and the high drop in strength. It is obvious that the impact strength follows a similar trend of reduction with temperature to the flexural strength, where both the flexural and impact strengths showed stable responses at 100 °C, followed by a continuous decrease until the approximate fading of the strength at 600 °C. This might be attributed to the type of stresses caused by the repeated impacts on the concrete, where the received impact forces tend to cause a fracture surface and then transfer this into tensile stresses that try to open the cracks until breakage failure. The higher strength reduction can also be attributed to the nature of the impact loads, where a sudden concentrated loading is induced within a very short time, leading to a higher stress concentration and hence a faster deterioration. As soon as the microstructure is internally fractured by the initiation of microcracks, only a few further concentrated drops are required to induce the surface cracking and failure of the specimen. Since the microstructure of the cement paste, the aggregate particles and the bond between them are negatively affected by the preceding heating phase of the specimens, a quick fracture of these specimens is expected under impact drops.

Figure 12 compares the behaviors of the residual impact strength in terms of the impact numbers of the disc specimens and the percentage weight loss of the same specimens. It can be said that the trend of the impact strength reduction is related to that of the percentage weight loss, where the same minor reduction is clear in the figure after exposure to 100 °C for both the strength and the weight loss, followed by a steep drop from 100 to 200 °C. After, a continuous decrease in the strength and an increase in weight loss are obvious from 300 to 600 °C. Indeed, the percentage strength is much higher than the percentage weight loss at each temperature; however, the behavior of the reduction with the temperature increase is quite similar.

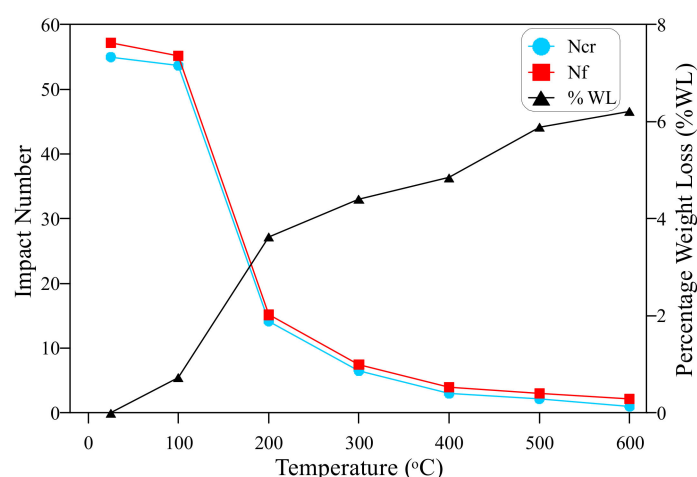


Figure 12. The relation of the impact number and percentage weight loss of the prism specimens at different temperatures.

As disclosed in the previous sections, the ACI 544-2R repeated impact test is known for its high variation in the obtained impact results. Figure 13 shows the effect of high temperature exposure on the variation in the cracking and failure impact numbers in terms of the coefficient of variation (COV). It is clear in the figure that the COV was not so high

(22.8) at ambient temperature, which is a good indication of the better control on the loading parameters using the automatic machine compared to the standard manual apparatus. The COV increased at 100 and 200 °C, recording values in the range of 41.4 and 44.8% for both the cracking and failure numbers. This increase in the result variation can be attributed to the dramatic behaviors at these temperatures, where at 100 °C, the specimens exhibited an increase and a decrease in strength compared to those tested at ambient temperature, as listed in Table 2. Similarly, the high drop in the impact number records at 200 °C resulted in high percentage variations, although there were limited numeral variations. The extremely low records of the impact numbers at the higher temperatures reduced the differences between the tested specimens, which, in turn, reduced the COV, as shown in Figure 13.

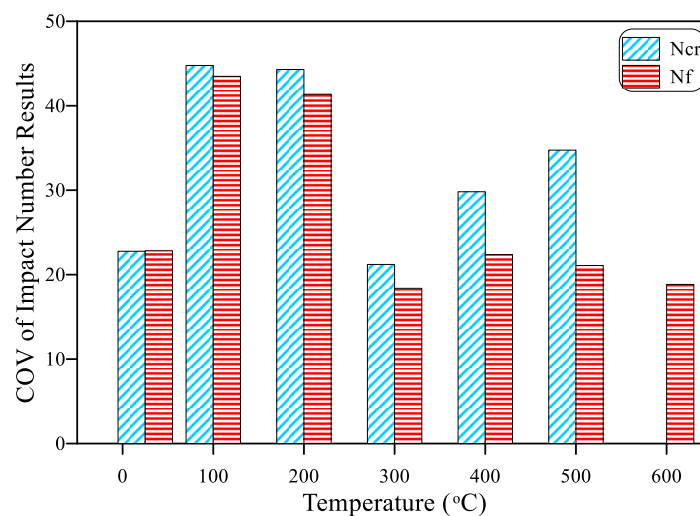


Figure 13. Coefficient of variation of the cracking and failure impact numbers at different temperatures.

3.3.2. Failure Patterns

Pictures for the disc specimens at room ambient temperature (R) and after exposure to 100, 200, 300, 400, 500 and 600 °C are shown in Figure 14a–g, both before and after impact testing. The fracture and failure of the reference unheated specimens align with what has been reported in previous studies [84–88] for plain concrete, where after a number of repeated blows, a small-diameter central fracture zone was created under the concentrated compression impacts via the top surface’s steel ball. After a few more blows, the internal cracks propagated to the surface, forming a surface cracking of two or three radial cracks from the central fracture zone, which formed the failure shape that occurred after a few additional blows, as shown in Figure 14a.

Figure 14b–d show that the specimens heated up to 300 °C exhibited a similar cracking and fracture behavior to that of the unheated specimens. However, at 200 and 300 °C, the cracking and failure tended to be softer, where the fracture started at much lower impact numbers, and the central fracture zone was smaller. The fracture of the specimens heated to temperatures above 400 °C is different. The material became so weak and absorbed the applied impact energy after being heated, where the cement paste became softer, the crushing strength of the aggregate particle reduced and the bond between them was almost lost. Due to these effects, internal thermal cracks were formed in the whole volume of the specimens. Therefore, for the specimens exposed to 400, 500 and 600 °C, only three impacts, two impacts and one impact were enough to cause the already existing cracks to appear at the surface. As a result, the central fracture zone was barely formed, and a higher number of major cracks (four or five) were formed accompanied by more hair cracks, as shown in Figure 14e–g.

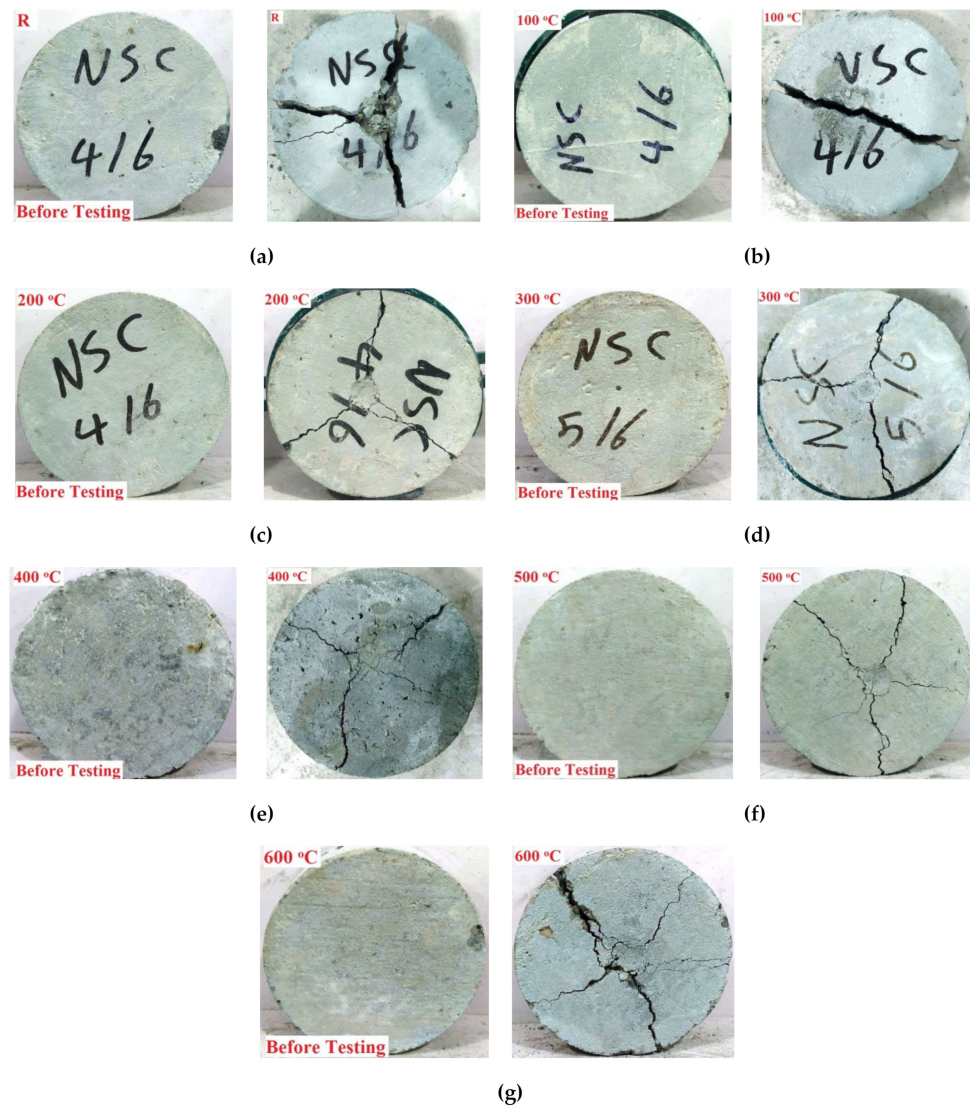


Figure 14. Failure patterns of the impact disc specimens at different temperatures (a) ambient temperature; (b): 100 °C; (c): 200 °C; (d) 300 °C; (e) 400 °C; (f) 500 °C; (g): 600 °C.

4. Weibull Distribution

At first, probabilistic methods were used to provide a rationale for the scattering of fracture strength results with a brittle nature. This statistical method has most widely been used to assess the statistical variability of impact test results in recent times [7,9,89]. Barbero et al. [90] investigated the mechanical properties of composite materials using the Weibull distribution. The authors recommended that the Weibull distribution is a pragmatic approach for determining 90% and 95% reliability values. The Weibull distribution is accentuated by two parameters, namely, shape and scale, and these parameters can be evaluated by several methods [91]. The scattering of the failure impact number of concretes was modeled using a two-parameter Weibull distribution. Lastly, the reliability of the concrete in terms of the failure impact number was presented in graphical form. The scattering of the cracking impact numbers was minor and hence was not modeled using the Weibull distribution.

4.1. Mean Standard Deviation Method (MSDM)

This method is more useful when the means and standard deviations are known; if this occurs, the shape parameter (α) and scale parameter (β) are determined using Equations (1) and (2) as follows [92].

$$\alpha = \left(\frac{\sigma}{\overline{N}_f} \right)^{-1.086} \quad (1)$$

$$\beta = \frac{\overline{R} \alpha^{2.6674}}{0.184 + 0.816 \alpha^{2.73855}} \quad (2)$$

where \overline{N}_f is the mean of the failure impact number, and σ is the standard deviation.

4.2. Energy Pattern Factor Method (EPFM)

The EPF is defined by the ratio of the summation of cubes of individual failure impact numbers to the cube of the mean failure impact number. The scale and shape parameters are calculated using Equations (3) and (4) once the EPF value is known [93].

$$EPF = \frac{\overline{N}_f^3}{\overline{N}_f^3} \quad (3)$$

$$\alpha = 1 + \frac{3.69}{(EPF)^2} \quad (4)$$

The gamma function is defined in Equation (5), expressed as follows.

$$\Gamma(x) = \int_0^{\infty} t^{x-1} \exp(-t) dt \quad (5)$$

4.3. Method of Moments (MOM)

Numerical iteration is involved in this method, and the mean failure impact number and corresponding standard deviation (σ) are used to find the shape and scale parameters [51].

$$\alpha = \left(\frac{0.9874}{\frac{\sigma}{\overline{R}}} \right)^{-1.086} \quad (6)$$

$$\overline{N}_f = \beta \Gamma(1 + 1/\alpha) \quad (7)$$

Table 3 demonstrates the results of the Weibull parameters obtained from three methods of distribution. It is clear from the table that the MSDM and MOM methods showed approximately the same parameter values. However, EPFM showed a lower value compared to MSDM and MOM. To perform the reliability analysis, the mean value of the three methods was used. The reliability of concrete exposed to various temperatures in terms of the failure impact number can be calculated using Equation (8) [94–98].

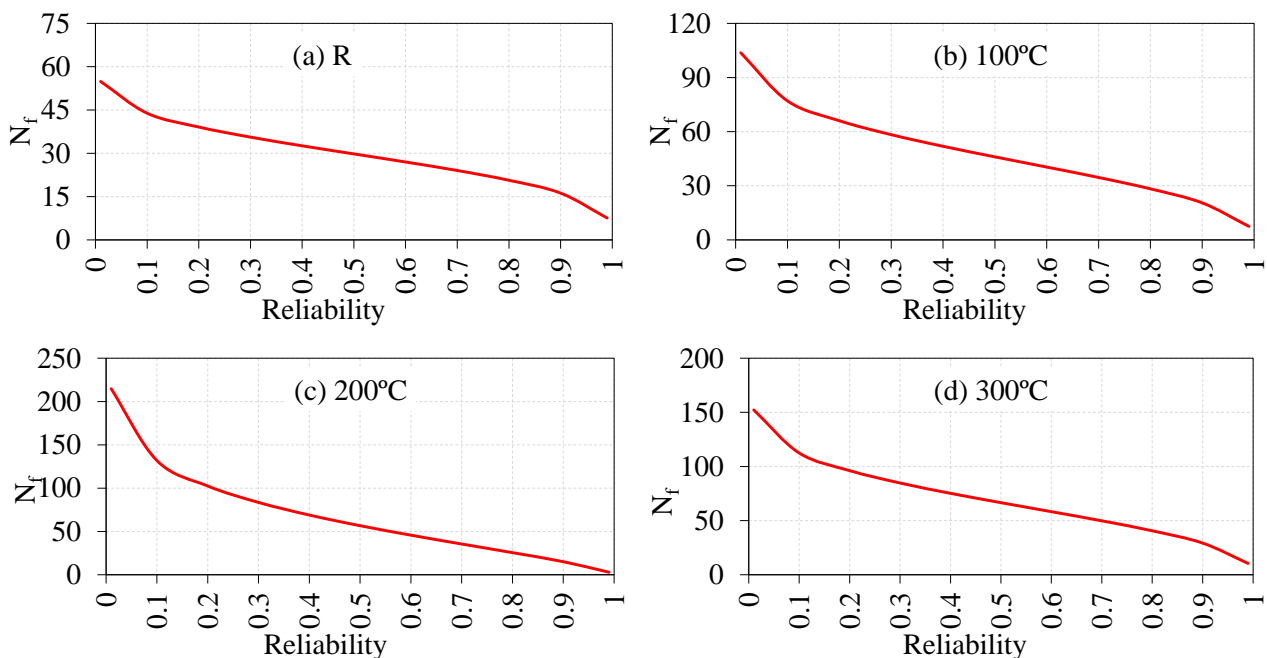
$$N_f = \beta (-\ln(R_x))^{(1/\alpha)} \quad (8)$$

where R_x is the reliability level, and R is the failure impact number.

Table 3. Results of Weibull parameters (scale and shape parameters).

Temperature	MSDM		EPFM		MOM		Mean	
	α	β	α	β	α	β	α	β
R	5.00	62.34	3.96	63.15	5.02	62.29	4.66	62.59
100 °C	2.47	62.25	2.80	61.99	2.46	62.24	2.58	62.16
200 °C	2.60	17.12	2.88	17.05	2.59	17.12	2.69	17.10
300 °C	6.19	8.06	4.23	8.25	6.23	8.07	5.55	8.13
400 °C	5.05	4.36	4.01	4.41	5.08	4.35	4.71	4.37
500 °C	5.74	3.24	4.08	3.31	5.78	3.24	5.20	3.26
600 °C	6.37	2.36	4.40	2.41	6.41	2.36	5.73	2.38

Using the Weibull parameters (mean values from Table 3), the reliability analysis was performed to estimate the failure impact number. Figure 15 illustrates the failure impact number in terms of the reliability or survival probability. By examining the 0.99 reliability (1% probability of failure), the failure impact numbers for the 100, 200, 300, 400, 500 and 600 °C specimens were 23, 10, 3, 4, 2, 1 and 1, respectively. By examining another probability level of 0.9 (10% probability of failure), the failure impact numbers were 39, 26, 7, 5, 3, 2 and 2, corresponding to the 100, 200, 300, 400, 500 and 600 °C specimens, respectively. Likewise, the failure impact number for the concrete exposed to different temperatures can be obtained from Figure 15. Using the reliability curves, the design engineer has the option to choose the required failure impact number at the desired reliability level (0.5 to 0.99). These values can be used effectively in the design calculations, and the Weibull distribution can be considered as a powerful tool to examine the scattering of the impact strength results. This statistical method and the outcomes are in good agreement with earlier studies [99–103].

**Figure 15.** Cont.

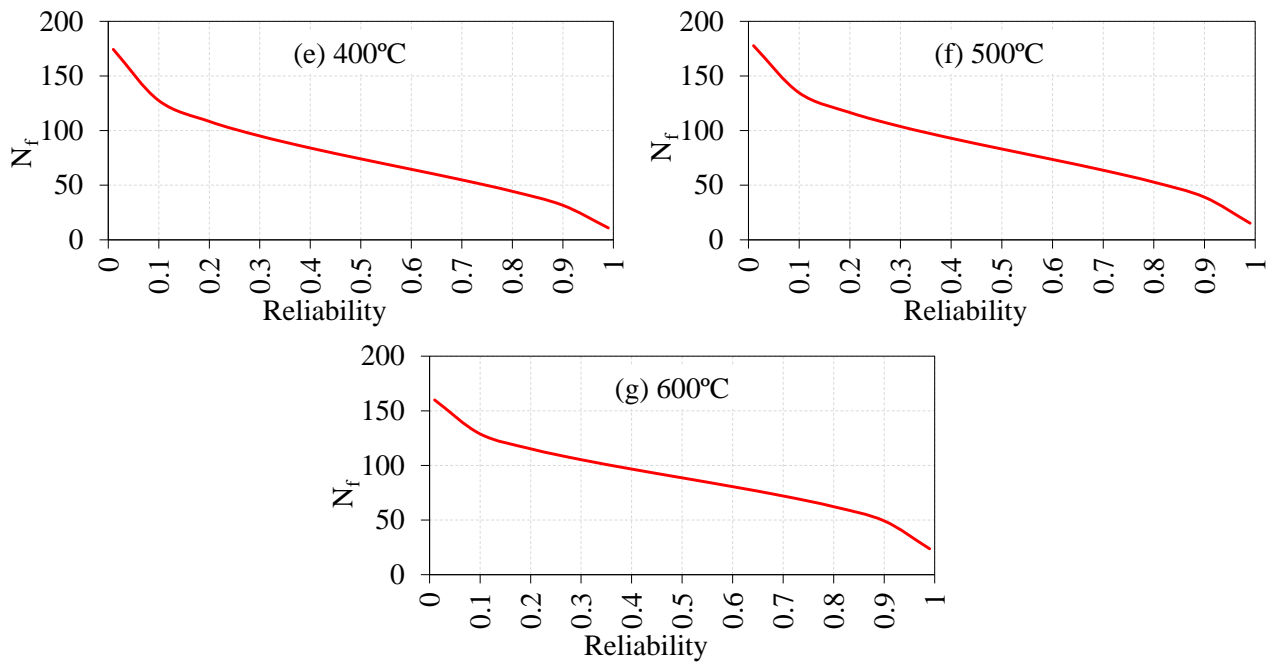


Figure 15. Failure number in terms of reliability (a) ambient temperature; (b): 100 °C; (c): 200 °C; (d) 300 °C; (e) 400 °C; (f) 500 °C; (g): 600 °C.

5. Conclusions

Based on the obtained experimental results from the study presented in this work, the following points are the most important conclusions.

1. The compressive strength was increased by less than 2% after exposure to 100 °C, while it decreased by more than 18% after exposure to 200 °C, followed by a partially recovered strength recorded at 300 °C. Finally, the compressive strength exhibited a continuous decrease after 400 °C, reaching a residual strength of approximately 50% of the original strength at 600 °C. This multi-phase behavior is attributed to the early loss of free water, physical and chemical changes in the cement paste after and the different thermal movements of the cement paste and aggregate.
2. Owing to the weak microstructural response of concrete under tensile stresses, the deterioration of the flexural strength after 200 °C was significantly higher than compressive strength, where the residual tensile strength after exposure to 400, 500 and 600 °C was approximately 58, 43 and 9%, respectively.
3. The impact strength, in terms of the cracking and failure impact numbers, was almost unaffected after exposure to 100 °C, where the reduction was only 2.4 and 3.5% in the cracking and failure numbers. However, a sharp drop in the impact strength of 74.2% was recorded after exposure to 200 °C, which was followed by a continuous decrease after exposure to the higher temperatures. The impact strength almost vanished at 600 °C, where the percentage reductions in the cracking and failure numbers were 98.2 and 96.2%, respectively. The higher strength drop under impact loads, compared to the compressive and tensile strengths, is attributed to the high concentrated tensile stresses induced in the material within a short time under the repeated impacts.
4. Comparing the residual strength with the percentage weight loss of the cube, prism and disc specimens, it was found that, by excluding the full or partial recovery regions, the strength follows an approximately similar behavior to that of weight loss after high temperature exposure. However, the percentage reduction in strength was much higher than the percentage increase in weight loss of the same specimens.
5. The failure of the specimens heated to temperatures up to 300 °C was similar to that of the unheated specimens, where a central fracture zone formed due to the concentrated compression impacts beneath the steel ball, followed by cracking and failure along

two or three radial cracks. On the other hand, the deteriorated microstructure of the specimens heated to temperatures of 400 to 600 °C imposed a different fracture behavior, where the specimens cracked quickly and softly along four or five paths accompanied by additional surface hair cracks, which reflects the weak strength of the material and the existence of internal thermal cracks prior to testing.

6. A rational distribution is desirable from a statistical perspective, in line with the relevant impact strength and, most significantly, with the safety of the design calculation. The Weibull distribution was found to be an efficient tool to examine the scattered test results and present the impact strength at the desired levels of reliability.

Author Contributions: Conceptualization, S.R.A.; methodology, S.H.A. and S.R.A.; software, G.M.; validation, S.R.A. and M.Ö.; formal analysis, G.M.; investigation, R.A.A.-A.; resources, R.A.A.-A.; data curation, S.R.A. and R.A.A.-A.; writing—original draft preparation, S.R.A., G.M. and R.A.A.-A.; writing—review and editing, M.Ö.; visualization, S.R.A. and S.H.A.; supervision, S.R.A. and M.Ö.; project administration, S.R.A. and M.Ö.; funding acquisition, S.R.A. and R.A.A.-A. All authors have read and agreed to the published version of the manuscript.

Funding: This research received no external funding.

Data Availability Statement: Not applicable.

Acknowledgments: The authors acknowledge the support from Al-Sharq Lab., Kut, Wasit, Iraq, and Ahmad A. Abbas.

Conflicts of Interest: The authors declare no conflict of interest.

References

1. Nili, M.; Afroughsabet, V. Combined effect of silica fume and steel fibers on the impact resistance and mechanical properties of concrete. *Int. J. Impact Eng.* **2010**, *37*, 879–886. [\[CrossRef\]](#)
2. Wang, W.; Chouw, N. The behavior of coconut fibre reinforced concrete (CFRC) under impact loading. *Constr. Build. Mater.* **2017**, *134*, 452–461. [\[CrossRef\]](#)
3. Abid, S.R.; Gunasekaran, M.; Ali, S.H.; Kadhum, A.L.; Al-Gasham, T.S.; Fediuk, R.; Vatin, N.; Karelina, M. Impact Performance of Steel Fiber-Reinforced Self-Compacting Concrete against Repeated Drop Weight Impact. *Crystals* **2021**, *11*, 91. [\[CrossRef\]](#)
4. Jabir, H.A.; Abid, S.R.; Murali, G.; Ali, S.H.; Klyuev, S.; Fediuk, R.; Vatin, N.; Promakhov, V.; Vasilev, Y. Experimental Tests and Reliability Analysis of the Cracking Impact Resistance of UHPFRC. *Fibers* **2020**, *8*, 74. [\[CrossRef\]](#)
5. Salaimanimagudam, M.P.; Suribabu, C.R.; Murali, G.; Abid, S.R. Impact Response of Hammerhead Pier Fibrous Concrete Beams Designed with Topology Optimization. *Period. Polytech. Civ. Eng.* **2020**, *64*, 1244–1258. [\[CrossRef\]](#)
6. ACI 544-2R. *Measurement of Properties of Fiber Reinforced Concrete*; American Concrete Institute: Indianapolis, IN, USA, 1999.
7. Haridharan, M.; Matheswaran, S.; Murali, G.; Abid, S.R.; Fediuk, R.; Amran, Y.M.; Abdelgader, H.S. Impact response of two-layered grouted aggregate fibrous concrete composite under falling mass impact. *Constr. Build. Mater.* **2020**, *263*, 120628. [\[CrossRef\]](#)
8. Murali, G.; Abid, S.R.; Amran, Y.M.; Abdelgader, H.S.; Fediuk, R.; Susrutha, A.; Poonguzhali, K. Impact performance of novel multi-layered prepacked aggregate fibrous composites under compression and bending. *Structures* **2020**, *28*, 1502–1515. [\[CrossRef\]](#)
9. Murali, G.; Abid, S.R.; Karthikeyan, K.; Haridharan, M.; Amran, M.; Siva, A. Low-velocity impact response of novel prepacked expanded clay aggregate fibrous concrete produced with carbon nano tube, glass fiber mesh and steel fiber. *Constr. Build. Mater.* **2021**, *284*, 122749. [\[CrossRef\]](#)
10. Imbabi, M.S.; Carrigan, C.; McKenna, S. Trends and developments in green cement and concrete technology. *Int. J. Sustain. Built Environ.* **2012**, *1*, 194–216. [\[CrossRef\]](#)
11. Sharma, N.K.; Kumar, P.; Kumar, S.; Thomas, B.S.; Gupta, R.C. Properties of concrete containing polished granite waste as partial substitution of coarse aggregate. *Constr. Build. Mater.* **2017**, *151*, 158–163. [\[CrossRef\]](#)
12. Babalola, O.; Awoyera, P.O.; Le, D.-H.; Romero, L.B. A review of residual strength properties of normal and high strength concrete exposed to elevated temperatures: Impact of materials modification on behaviour of concrete composite. *Constr. Build. Mater.* **2021**, *296*, 123448. [\[CrossRef\]](#)
13. Gagg, C.R. Cement and concrete as an engineering material: An historic appraisal and case study analysis. *Eng. Fail. Anal.* **2014**, *40*, 114–140. [\[CrossRef\]](#)
14. Behera, M.; Bhattacharyya, S.K.; Minocha, A.K.; Deoliya, R.; Maiti, S. Recycled aggregate from C&D waste & its use in concrete—A break through towards sustainability in construction sector: A review. *Constr. Build. Mater.* **2014**, *68*, 501–516.
15. Tufail, M.; Shahzada, K.; Gencturk, B.; Wei, J. Effect of Elevated Temperature on Mechanical Properties of Limestone, Quartzite and Granite Concrete. *Int. J. Concr. Struct. Mater.* **2016**, *11*, 17–28. [\[CrossRef\]](#)

16. Arna'Ot, F.H.; Abid, S.R.; Özakça, M.; Tayşi, N. Review of concrete flat plate-column assemblies under fire conditions. *Fire Saf. J.* **2017**, *93*, 39–52. [[CrossRef](#)]
17. Guo, Y.-C.; Zhang, J.-H.; Chen, G.-M.; Xie, Z.-H. Compressive behaviour of concrete structures incorporating recycled concrete aggregates, rubber crumb and reinforced with steel fibre, subjected to elevated temperatures. *J. Clean. Prod.* **2014**, *72*, 193–203. [[CrossRef](#)]
18. Mehdipour, S.; Nikbin, I.; Dezhampanah, S.; Mohebbi, R.; Moghadam, H.; Charkhtab, S.; Moradi, A. Mechanical properties, durability and environmental evaluation of rubberized concrete incorporating steel fiber and metakaolin at elevated temperatures. *J. Clean. Prod.* **2020**, *254*, 120126. [[CrossRef](#)]
19. Alimrani, N.; Balazs, G.L. Investigations of direct shear of one-year old SFRC after exposed to elevated temperatures. *Constr. Build. Mater.* **2020**, *254*, 119308. [[CrossRef](#)]
20. Drzymala, T.; Jackiewicz-Rek, W.; Tomaszewski, M.; Kuś, A.; Gałaj, J.; Śukys, R. Effects of high temperatures on the properties of high performance concrete (HPC). *Procedia Eng.* **2017**, *172*, 256–263. [[CrossRef](#)]
21. Chu, H.-Y.; Jiang, J.-Y.; Sun, W.; Zhang, M. Mechanical and physicochemical properties of ferro-siliceous concrete subjected to elevated temperatures. *Constr. Build. Mater.* **2016**, *122*, 743–752. [[CrossRef](#)]
22. Roufael, G.; Beaucour, A.-L.; Eslami, J.; Hoxha, D.; Noumowé, A. Influence of lightweight aggregates on the physical and mechanical residual properties of concrete subjected to high temperatures. *Constr. Build. Mater.* **2020**, *268*, 121221. [[CrossRef](#)]
23. Deng, Z.; Huang, H.; Ye, B.; Wang, H.; Xiang, P. Investigation on recycled aggregate concretes exposed to high temperature by biaxial compressive tests. *Constr. Build. Mater.* **2020**, *244*, 118048. [[CrossRef](#)]
24. Phan, L.T.; Carino, N.J. Code provisions for high strength concrete strength-temperature relationship at elevated temperatures. *Mater. Struct.* **2003**, *36*, 91–98. [[CrossRef](#)]
25. Phan, L.T.; Carino, N.J. Review of Mechanical Properties of HSC at Elevated Temperature. *J. Mater. Civ. Eng.* **1998**, *10*, 58–65. [[CrossRef](#)]
26. Husem, M. The effects of high temperature on compressive and flexural strengths of ordinary and high-performance concrete. *Fire Saf. J.* **2006**, *41*, 155–163. [[CrossRef](#)]
27. Chen, L.; Fang, Q.; Jiang, X.; Ruan, Z.; Hong, J. Combined effects of high temperature and high strain rate on normal weight concrete. *Int. J. Impact Eng.* **2015**, *86*, 40–56. [[CrossRef](#)]
28. Zhai, C.; Chen, L.; Xiang, H.; Fang, Q. Experimental and numerical investigation into RC beams subjected to blast after exposure to fire. *Int. J. Impact Eng.* **2016**, *97*, 29–45. [[CrossRef](#)]
29. Zhai, C.; Chen, L.; Fang, Q.; Chen, W.; Jiang, X. Experimental study of strain rate effects on normal weight concrete after exposure to elevated temperature. *Mater. Struct.* **2016**, *50*, 40. [[CrossRef](#)]
30. Mirmomeni, M.; Heidarpour, A.; Zhao, X.-L.; Packer, J.A. Effect of elevated temperature on the mechanical properties of high-strain-rate-induced partially damaged concrete and CFSTs. *Int. J. Impact Eng.* **2017**, *110*, 346–358. [[CrossRef](#)]
31. Kakogiannis, D.; Pascualena, F.; Reymen, B.; Pyl, L.; Ndambi, J.M.; Segers, E.; Lecompte, D.; Vantomme, J.; Krauthammer, T. Blast performance of reinforced concrete hollow core slabs in combination with fire: Numerical and experimental assessment. *Fire Saf. J.* **2013**, *57*, 69–82. [[CrossRef](#)]
32. Jin, L.; Bai, J.; Zhang, R.; Li, L.; Du, X. Effect of elevated temperature on the low-velocity impact performances of reinforced concrete slabs. *Int. J. Impact Eng.* **2021**, *149*, 103797. [[CrossRef](#)]
33. Pan, L.; Chen, L.; Fang, Q.; Zhai, C. A modified layered-section method for responses of fire-damaged reinforced concrete beams under static and blast loads. *Int. J. Prot. Struct.* **2016**, *7*, 495–517. [[CrossRef](#)]
34. Yu, X.; Chen, L.; Fang, Q.; Ruan, Z.; Hong, J.; Xiang, H. A concrete constitutive model considering coupled effects of high temperature and high strain rate. *Int. J. Impact Eng.* **2017**, *101*, 66–77. [[CrossRef](#)]
35. Jin, L.; Lan, Y.; Zhang, Z.; Du, X. Impact performances of RC beams at/after elevated temperature: Ameso-scale study. *Eng. Fail. Anal.* **2019**, *105*, 196–214. [[CrossRef](#)]
36. Arioz, O. Retained properties of concrete exposed to high temperatures: Size effect. *Fire Mater.* **2009**, *33*, 211–222. [[CrossRef](#)]
37. Erdem, T.K. Specimen size effect on the residual properties of engineered cementitious composites subjected to high temperatures. *Cem. Concr. Compos.* **2014**, *45*, 1–8. [[CrossRef](#)]
38. Chan, W.; Luo, Y.N.; Sun, X. Compressive strength and pore structure of high performance concrete after exposure to high temperature up to 800 °C. *Cem. Concr. Res.* **2000**, *30*, 247–251. [[CrossRef](#)]
39. Xu, Y.; Wong, Y.; Poon, C.S.; Anson, M. Impact of high temperature on PFA concrete. *Cem. Concr. Res.* **2001**, *31*, 1065–1073. [[CrossRef](#)]
40. Poon, C.S.; Azhar, S.; Anson, M.; Wong, Y.-L. Comparison of the strength and durability performance of normal- and high-strength pozzolanic concretes at elevated temperatures. *Cem. Concr. Res.* **2001**, *31*, 1291–1300. [[CrossRef](#)]
41. Netinger, I.; Kesegic, I.; Guljas, I. The effect of high temperatures on the mechanical properties of concrete made with different types of aggregates. *Fire Saf. J.* **2011**, *46*, 425–430. [[CrossRef](#)]
42. Rashad, A.M. Potential Use of Silica Fume Coupled with Slag in HVFA Concrete Exposed to Elevated Temperatures. *J. Mater. Civ. Eng.* **2015**, *27*, 4015019. [[CrossRef](#)]
43. Malik, M.; Bhattacharyya, S.K.; Barai, S.V. Microstructural Changes in Concrete: Postfire Scenario. *J. Mater. Civ. Eng.* **2021**, *33*, 4020462. [[CrossRef](#)]

44. Hager, I.; Tracz, T.; Choin´ska, M.; Mróz, K. Effect of cement type on the mechanical behavior and permeability of concrete subjected to high temperatures. *Materials* **2019**, *12*, 3021. [[CrossRef](#)] [[PubMed](#)]
45. Li, Y.; Tan, K.H.; Yang, E.-H. Synergistic effects of hybrid polypropylene and steel fibers on explosive spalling prevention of ultra-high performance concrete at elevated temperature. *Cem. Concr. Compos.* **2018**, *96*, 174–181. [[CrossRef](#)]
46. Yonggui, W.; Shuaipeng, L.; Hughes, P.; Yuhui, F. Mechanical properties and microstructure of basalt fibre and nano-silica reinforced recycled concrete after exposure to elevated temperatures. *Constr. Build. Mater.* **2020**, *247*, 118561. [[CrossRef](#)]
47. Lau, A.; Anson, M. Effect of high temperatures on high performance steel fibre reinforced concrete. *Cem. Concr. Res.* **2006**, *36*, 1698–1707. [[CrossRef](#)]
48. Düğenci, O.; Haktanir, T.; Altun, F. Experimental research for the effect of high temperature on the mechanical properties of steel fiber-reinforced concrete. *Constr. Build. Mater.* **2015**, *75*, 82–88. [[CrossRef](#)]
49. Da Silva, J.B.; Pepe, M.; Filho, R.D.T. High temperatures effect on mechanical and physical performance of normal and high strength recycled aggregate concrete. *Fire Saf. J.* **2020**, *117*, 103222. [[CrossRef](#)]
50. Mathews, M.E.; Kiran, T.; Naidu, V.C.H.; Jeyakumar, G.; Anand, N. Effect of high-temperature on the mechanical and durability behaviour of concrete. *Mater. Today: Proc.* **2020**, *42*, 718–725. [[CrossRef](#)]
51. Al-Owaisy, S.R. Effect of high temperatures on shear transfer strength of concrete. *J. Eng. Sustain. Dev.* **2007**, *11*, 92–103.
52. Tang, C.-W. Residual Mechanical Properties of Fiber-Reinforced Lightweight Aggregate Concrete after Exposure to Elevated Temperatures. *Appl. Sci.* **2020**, *10*, 3519. [[CrossRef](#)]
53. Zhang, B.; Bicanic, N.; Pearce, C.J.; Balabanic, G.; Purkiss, J.A. Discussion: Residual fracture properties of normal- and high-strength concrete subject to elevated temperatures. *Mag. Concr. Res.* **2000**, *52*, 123–136. [[CrossRef](#)]
54. Yermak, N.; Pliya, P.; Beaucour, A.-L.; Simon, A.; Noumowé, A. Influence of steel and/or polypropylene fibres on the behaviour of concrete at high temperature: Spalling, transfer and mechanical properties. *Constr. Build. Mater.* **2017**, *132*, 240–250. [[CrossRef](#)]
55. Pliya, P.; Beaucour, A.-L.; Noumowé, A. Contribution of cocktail of polypropylene and steel fibres in improving the behaviour of high strength concrete subjected to high temperature. *Constr. Build. Mater.* **2010**, *25*, 1926–1934. [[CrossRef](#)]
56. Ahmad, S.; Rasul, M.; Adekunle, S.K.; Al-Dulaijan, S.U.; Maslehuddin, M.; Ali, S.I. Mechanical properties of steel fiber-reinforced UHPC mixtures exposed to elevated temperature: Effects of exposure duration and fiber content. *Compos. Part B Eng.* **2018**, *168*, 291–301. [[CrossRef](#)]
57. Wu, H.; Lin, X.; Zhou, A. A review of mechanical properties of fibre reinforced concrete at elevated temperatures. *Cem. Concr. Res.* **2020**, *135*, 106117. [[CrossRef](#)]
58. Khaliq, W.; Kodur, V. Thermal and mechanical properties of fiber reinforced high performance self-consolidating concrete at elevated temperatures. *Cem. Concr. Res.* **2011**, *41*, 1112–1122. [[CrossRef](#)]
59. Khaliq, W.; Kodur, V. High temperature mechanical properties of high-strength fly ash concrete with and without fibers. *ACI Mater. J.* **2012**, *109*, 665–674.
60. Ju, Y.; Wang, L.; Liu, H.; Tian, K. An experimental investigation of the thermal spalling of polypropylene-fibered reactive powder concrete exposed to elevated temperatures. *Sci. Bull.* **2015**, *60*, 2022–2040. [[CrossRef](#)]
61. Caetano, H.; Ferreira, G.; Rodrigues, J.P.C.; Pimienta, P. Effect of the high temperatures on the microstructure and compressive strength of high strength fibre concretes. *Constr. Build. Mater.* **2018**, *199*, 717–736. [[CrossRef](#)]
62. Zheng, W.; Li, H.; Wang, Y. Compressive behaviour of hybrid fiber-reinforced reactive powder concrete after high temperature. *Mater. Des.* **2012**, *41*, 403–409. [[CrossRef](#)]
63. Raza, S.S.; Qureshi, L.A. Effect of carbon fiber on mechanical properties of reactive powder concrete exposed to elevated temperatures. *J. Build. Eng.* **2021**, *42*, 102503. [[CrossRef](#)]
64. Luo, X.; Sun, W.; Nin Chan, S.Y. Effect of heating and cooling regimes on residual strength and microstructure of normal strength and high-performance concrete. *Cem. Concr. Res.* **2000**, *30*, 379–383. [[CrossRef](#)]
65. Sideris, K.K.; Manita, P. Residual mechanical characteristics and spalling resistance of fiber reinforced self-compacting concretes exposed to elevated temperatures. *Constr. Build. Mater.* **2013**, *41*, 296–302. [[CrossRef](#)]
66. Zhang, D.; Dasari, A.; Tan, K.H. On the mechanism of prevention of explosive spalling in ultra-high performance concrete with polymer fibers. *Cem. Concr. Res.* **2018**, *113*, 169–177. [[CrossRef](#)]
67. Aslani, F.; Keli, J. Assessment and development of high-performance fibre-reinforced lightweight self-compacting concrete including recycled crumb rubber aggregates exposed to elevated temperatures. *J. Clean. Prod.* **2018**, *200*, 1009–1025. [[CrossRef](#)]
68. Eidan, J.; Rasoolan, I.; Rezaeian, A.; Poorveis, D. Residual mechanical properties of polypropylene fiber-reinforced concrete after heating. *Constr. Build. Mater.* **2018**, *198*, 195–206. [[CrossRef](#)]
69. Peng, G.-F.; Yang, W.-W.; Zhao, J.; Liu, Y.-F.; Bian, S.-H.; Zhao, L.-H. Explosive spalling and residual mechanical properties of fiber-toughened high-performance concrete subjected to high temperatures. *Cem. Concr. Res.* **2006**, *36*, 723–727. [[CrossRef](#)]
70. Gao, D.; Yan, D.; Li, X. Splitting strength of GGBFS concrete incorporating with steel fiber and polypropylene fiber after exposure to elevated temperatures. *Fire Saf. J.* **2012**, *54*, 67–73. [[CrossRef](#)]
71. Canbaz, M. The effect of high temperature on reactive powder concrete. *Constr. Build. Mater.* **2014**, *70*, 508–513. [[CrossRef](#)]
72. Sultan, H.K.; Alyaseri, I. Effects of elevated temperatures on mechanical properties of reactive powder concrete elements. *Constr. Build. Mater.* **2020**, *261*, 120555. [[CrossRef](#)]
73. Arna'Ot, F.H.; Abbass, A.A.; Abualtemen, A.A.; Abid, S.R.; Özakaça, M. Residual strength of high strength concentric column-SFRC flat plate exposed to high temperatures. *Constr. Build. Mater.* **2017**, *154*, 204–218. [[CrossRef](#)]

74. Al-Owaisy, S.R. Strength and elasticity of steel fiber reinforced concrete at high temperatures. *J. Eng. Sustain. Dev.* **2007**, *11*, 125–133.
75. Torić, N.; Boko, I.; Peros, B. Reduction of Postfire Properties of High-Strength Concrete. *Adv. Mater. Sci. Eng.* **2013**, *2013*, 712953. [[CrossRef](#)]
76. Cheng, F.-P.; Kodur, V.K.R.; Wang, T.-C. Stress-Strain Curves for High Strength Concrete at Elevated Temperatures. *J. Mater. Civ. Eng.* **2004**, *16*, 84–90. [[CrossRef](#)]
77. Al-Owaisy, S.R. Post heat exposure properties of steel fiber reinforced concrete. *J. Eng. Sustain. Dev.* **2006**, *10*, 194–207.
78. Varona, F.B.; Baeza-Brotos, F.; Tenza-Abril, A.J.; Baeza, F.J.; Bañón, L. Residual Compressive Strength of Recycled Aggregate Concretes after High Temperature Exposure. *Materials* **2020**, *13*, 1981. [[CrossRef](#)]
79. Amin, M.N.; Khan, K. Mechanical Performance of High-Strength Sustainable Concrete under Fire Incorporating Locally Available Volcanic Ash in Central Harrat Rahat, Saudi Arabia. *Materials* **2020**, *14*, 21. [[CrossRef](#)]
80. Zhang, P.; Kang, L.; Wang, J.; Guo, J.; Hu, S.; Ling, Y. Mechanical Properties and Explosive Spalling Behavior of Steel-Fiber-Reinforced Concrete Exposed to High Temperature—A Review. *Appl. Sci.* **2020**, *10*, 2324. [[CrossRef](#)]
81. Ding, Y.; Li, D.; Zhang, Y.; Azevedo, C. Experimental investigation on the composite effect of steel rebars and macro fibers on the impact behavior of high performance self-compacting concrete. *Constr. Build. Mater.* **2017**, *136*, 495–505. [[CrossRef](#)]
82. Abid, S.R.; Abdul-Hussein, M.L.; Ayoob, N.S.; Ali, S.H.; Kadhum, A.L. Repeated drop-weight impact tests on self-compacting concrete reinforced with micro-steel fiber. *Heliyon* **2020**, *6*, e03198. [[CrossRef](#)]
83. Mastali, M.; Dalvand, A. The impact resistance and mechanical properties of self-compacting concrete reinforced with recycled CFRP pieces. *Compos. Part B Eng.* **2016**, *92*, 360–376. [[CrossRef](#)]
84. Nili, M.; Afroughsabet, V. The effects of silica fume and polypropylene fibers on the impact resistance and mechanical properties of concrete. *Constr. Build. Mater.* **2010**, *24*, 927–933. [[CrossRef](#)]
85. Abid, S.R.; Hussein, M.L.A.; Ali, S.H.; Kazem, A.F. Suggested modified testing techniques to the ACI 544-R repeated drop-weight impact test. *Constr. Build. Mater.* **2020**, *244*, 118321. [[CrossRef](#)]
86. Murali, G.; Abid, S.R.; Abdelgader, H.S.; Amran, Y.H.M.; Shekarchi, M.; Wilde, K. Repeated Projectile Impact Tests on Multi-Layered Fibrous Cementitious Composites. *Int. J. Civ. Eng.* **2021**, *19*, 635–651. [[CrossRef](#)]
87. Abid, S.R.; Murali, G.; Amran, M.; Vatin, N.; Fediuk, R.; Karelina, M. Evaluation of Mode II Fracture Toughness of Hybrid Fibrous Geopolymer Composites. *Materials* **2021**, *14*, 349. [[CrossRef](#)]
88. Murali, G.; Abid, S.; Amran, M.; Fediuk, R.; Vatin, N.; Karelina, M. Combined Effect of Multi-Walled Carbon Nanotubes, Steel Fibre and Glass Fibre Mesh on Novel Two-Stage Expanded Clay Aggregate Concrete against Impact Loading. *Crystals* **2021**, *11*, 720. [[CrossRef](#)]
89. Ramakrishnan, K.; Depak, S.; Hariharan, K.; Abid, S.R.; Murali, G.; Cecchin, D.; Fediuk, R.; Amran, Y.M.; Abdelgader, H.S.; Khatib, J.M. Standard and modified falling mass impact tests on preplaced aggregate fibrous concrete and slurry infiltrated fibrous concrete. *Constr. Build. Mater.* **2021**, *298*, 123857. [[CrossRef](#)]
90. Barbero, E.; Fernandez-Saez, J.; Navarro, C. Statistical analysis of the mechanical properties of composite materials. *Compos. Part B Eng.* **2000**, *31*, 375–381. [[CrossRef](#)]
91. Murali, G.; Indhumathi, T.; Karthikeyan, K.; Ramkumar, V.R. Analysis of flexural fatigue failure of concrete made with 100% coarse recycled and natural aggregates. *Comput. Concr.* **2018**, *21*, 291–298.
92. Mohammadi, K.; Alavi, O.; Mostafaeipour, A.; Goudarzi, N.; Jalilvand, M. Assessing different parameters estimation methods of Weibull distribution to compute wind power density. *Energy Convers. Manag.* **2016**, *108*, 322–335. [[CrossRef](#)]
93. Akdağ, S.A.; Dinler, A. A new method to estimate Weibull parameters for wind energy applications. *Energy Convers. Manag.* **2009**, *50*, 1761–1766. [[CrossRef](#)]
94. Murali, G.; Muthulakshmi, T.; Nycilin Karunya, N.; Iswarya, R.; Hannah Jennifer, G.; Karthikeyan, K. Impact Response and Strength Reliability of Green High-Performance Fibre Reinforced Concrete Subjected to Freeze-Thaw Cycles in NaCl Solution. *Mater. Sci. Medzg.* **2017**, *23*, 384–388.
95. Murali, G.; Santhi, A.S.; Ganesh, G.M. Impact Resistance and Strength Reliability of Fiber-reinforced Concrete in Bending under Drop Weight Impact Load. *Int. J. Technol.* **2014**, *5*, 111. [[CrossRef](#)]
96. Murali, G.; Santhi, A.S.; Mohan Ganesh, G. Impact resistance and strength reliability of fiber reinforced concrete using two parameter Weibull distribution. *ARPJ. J. Eng. Appl. Sci.* **2014**, *9*, 554–559.
97. Murali, G.; Gayathri, R.; Ramkumar, V.R.; Karthikeyan, K. Two statistical scrutinize of impact strength and strength reliability of steel Fibre-Reinforced Concrete. *KSCE J. Civ. Eng.* **2017**, *22*, 257–269. [[CrossRef](#)]
98. Murali, G.; Asrani, N.P.; Ramkumar, V.R.; Siva, A.; Haridharan, M.K. Impact Resistance and Strength Reliability of Novel Two-Stage Fibre-Reinforced Concrete. *Arab. J. Sci. Eng.* **2018**, *44*, 4477–4490. [[CrossRef](#)]
99. Asrani, N.P.; Murali, G.; Parthiban, K.; Surya, K.; Prakash, A.; Rathika, K.; Chandru, U. A feasibility of enhancing the impact resistance of hybrid fibrous geopolymer composites: Experiments and modelling. *Constr. Build. Mater.* **2019**, *203*, 56–68. [[CrossRef](#)]
100. Abirami, T.; Loganaganandan, M.; Murali, G.; Fediuk, R.; Sreekrishna, R.V.; Vignesh, T.; Janupriya, G.; Karthikeyan, K. Experimental research on impact response of novel steel fibrous concretes under falling mass impact. *Constr. Build. Mater.* **2019**, *222*, 447–457. [[CrossRef](#)]

101. Prasad, N.; Murali, G. Exploring the impact performance of functionally-graded preplaced aggregate concrete incorporating steel and polypropylene fibres. *J. Build. Eng.* **2021**, *35*, 102077. [[CrossRef](#)]
102. Murali, G.; Karthikeyan, K.; Ramkumar, V.R. Reliability Analysis of Impact Failure Energy of Fibre Reinforced Concrete Using Weibull Distribution. *J. Appl. Sci. Eng.* **2018**, *21*, 163–170.
103. Gayathri, R.; Murali, G.; Parthiban, K.; Haridharan, M.K.; Karthikeyan, K. A Four Novel Energy Pattern Factor Method for Computation of Weibull Parameter in Impact Strength Reliability of Fibre Reinforced Concrete. *Inter. J. Eng. Tech.* **2018**, *7*, 272–280.